ACS Catalysis

Research Article

pubs.acs.org/acscatalysis

Highly Selective Liquid-Phase Oxidation of Cyclohexane to KA Oil over Ti-MWW Catalyst: Evidence of Formation of Oxyl Radicals

Wen-Juan Zhou,[†,§] Raphael Wischert,[§] Kai Xue,[†] Yu-Ting Zheng,[∥] Belén Albela,[∥] Laurent Bonneviot,[∥] Jean-Marc Clacens,[§] Floryan De Campo,[§] Marc Pera-Titus,*[,§] and Peng Wu*[,†]

[†]Shanghai Key Laboratory of Green Chemistry and Chemical Processes, Department of Chemistry, East China Normal University, Shanghai, China

[§]Eco-Efficient Products and Processes Laboratory (E2P2L), UMI 3464 CNRS—Solvay, 3966 Jin Du Road, Xin Zhuang Ind. Zone, 201108 Shanghai, China

[∥]Laboratoire de Chimie, UMR 5182 CNRS—Ecole Normale Supérieure de Lyon, 46 allée d'Italie, 69364 Lyon, France

Supporting Information

ABSTRACT: Various types of Ti-containing zeolites, i.e., Ti-MWW, TS-1, Ti-MOR, and Ti-BEA, have been evaluated as candidates for the liquid-phase oxidation of cyclohexane using *t*-butyl hydroperoxide (TBHP, 7−8 wt %) as model oxidant. Ti-MWW zeolite displayed the highest activity for cyclohexanol and cyclohexanone (KA oil) with an overall selectivity higher than 90% at 80 °C, making this catalyst a candidate of choice for industrial KA oil production by deperoxidation of cyclohexyl hydroperoxide. The effect of the reaction temperature, reaction time, catalyst amount, and catalyst stability on Ti-MWW was surveyed in detail. The Ti-MWW catalyst showed a stable performance and could be recycled at least four times without detectable Ti leaching and loss of structural stability. The active sites for cyclohexane oxidation appeared to be located near external 12-ring cups in the Ti-MWW framework as suggested by a series of position-selective poisoning tests with tripropyl- and triphenylamine, impelling cyclohexane diffusion within the internal 10-ring channels. EPR experiments supported by DFT calculations suggested the coexistence of both Ti(IV)-OO• (peroxyl) and Ti(IV)-O• (oxyl) species generated through bimolecular pathways, implying simultaneously $(SiO)_3Ti(OOtBu)$ species and tBuOOH. The catalytic activity was strongly inhibited in the presence of alkenes, leading to the preferential formation of the epoxidation product with no detectable formation of radicals. Notably, this is the first time that oxyl species have been detected particularly with the help of DFT calculations. Predicted differences of *g* tensors between peroxyl and oxyl species at various hydration levels in the presence of cyclohexane were consistent with the EPR spectra.

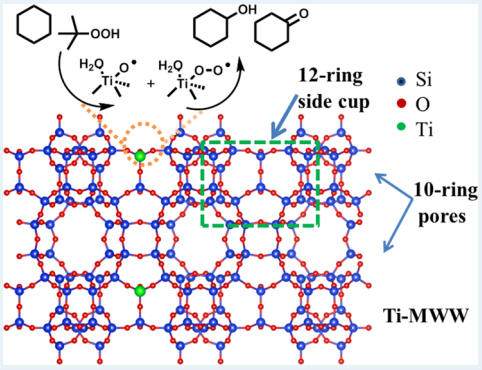

KEYWORDS: *cyclohexane, oxidation, Ti-MWW, titanosilicate, KA oil, oxyl radical*

1. INTRODUCTION

Cyclohexanol and cyclohexanone (the mixture is known as KA oil, production >200 kton/year) are readily oxidized to adipic acid, an important intermediate in the manufacture of condensation polymers, in particular polyamides such as Nylon-6.6.[1] KA oil is industrially produced by the partial oxidation of cyclohexane in a process involving two consecutive steps: (1) noncatalytic autoxidation of cyclohexane by oxygen to cyclohexyl hydroperoxide (CHHP), and (2) deperoxidation of CHHP to KA oil using a homogeneous Co(II) catalyst. However, this process suffers from significant shortcomings. In the first step, the selectivity for CHHP is only 60−70% with a very low cyclohexane conversion of 3−4%.[2,3] The need for recycling the unreacted cyclohexane leads to high operational costs. The second step is seriously flawed by environmental issues, since the Co(II) catalyst cannot be completely recovered and recycled, as it is easily discharged with salts leaving the process. In addition, each kilogram of KA oil requires about 180 kg of NaOH, generating in turn ca. 1100 kg of exhausted alkaline solution.

The above stated economical and environmental drawbacks of the KA oil process could be certainly mitigated by using a heterogeneous catalyst in the deperoxidation step (step 2). Indeed, catalytic formulations based on noble metals incorporated into oxides, zeolites, or aluminophosphates have shown high activities and selectivities for KA oil.[4−6] However, their high cost, combined with the rapid deactivation by metal leaching, acts as a deterrent for their implementation. Furthermore, other formulations based on transition metals (e.g., Cr, Cu, Co, Nb, Ta) only afforded modest yields.[7−12] The development of a catalyst with optimal selectivity for KA oil at

Received: August 30, 2013
Revised: November 8, 2013
Published: November 21, 2013

Table 1. Physicochemical Properties and Cyclohexane Oxidation Results of Various Titanosilicate Catalysts[a]

		specific surface (m^2/g)		Si/Ti ratio						turnover number (−)[b]	
catalyst	pore size (Å)	BET	external	Si/Ti_b (ICP)	Si/Ti_s (XPS)	TBHP Conv. %	sel. KA %	yield KA %	A/K	TON_b	TON_s
Ti-MWW-1	5.3, 7.0	435	132	49(51[c])	53	10.7	90.1	9.6	8.4	10.0	47.4
Ti-MWW-2	5.3, 7.0	425	129	67	92	14.1	49.1	6.9	15.6	7.7	44.5
TS-1	5.3	329	193	32	33	10.1	28.5	2.9	1.0	2.1	4.8
Ti-BEA	6.7	557	93	63	52	42.4	17.6	7.5	∞	9.7	
Ti-MOR	7.0			84		0.2	98.1	0.2	∞	1.5	

[a]Reaction conditions: 80 °C, 1.0 h, 0.10 g catalyst, 4 g of cyclohexane containing 7.7 wt % TBHP. [b]TON_b = KA yield (mol)/total Ti site (mol) in titanosilicate (1 h). TON_s = KA yield (mol)/external Ti site (mol) in titanosilicate (1 h). [c]After the reaction.

relatively low CHHP concentrations is still an unsolved challenge today.

Ti-containing zeolites with isomorphously substituted isolated Ti(IV) sites have shown promising potential in the mild oxidation of alkanes and alkenes.[13] In particular, Ti-silicalite (TS-1)[14] with medium-sized pore channels has been widely used for the epoxidation of short-chain alkenes and the hydroxylation of benzene and phenol using hydrogen peroxide as oxidant. In contrast, Ti-loaded zeolites with larger channels (e.g., Ti-BEA,[15−18] Ti-ZSM-12,[19] Ti-BEC,[20] Ti-MOR[21]), as well as mesoporous titanosilicates (e.g., Ti-MCM-41,[22−24] Ti-SBA-15,[24] Ti-SBA-16[25]) and more recently materials with hierarchical structures,[26−29] appear more adapted for the oxidation of bulky aryls and aromatics using either hydrogen peroxide or organic hydroperoxides.

Despite the anticipated benefits of large-pore titanosilicates for CHHP deperoxidation, significant drawbacks prevent their industrial use. First, most of these materials suffer from strong deactivation due to Ti-leaching during operation. Second, the dispersion of Ti sites is often more difficult to control than for TS-1, requiring a fine balance of the hydrolysis rates of the Ti and Si precursors and a complete removal of Al and other impurities during hydrothermal synthesis.[14,30] Moreover, specific postsynthesis techniques for grafting in mesopores,[31] or dealumination/titanation in some zeolites have been proposed.[32,33] Third, unlike TS-1, these materials usually exhibit a prominent hydrophilic behavior due to the abundant presence of silanol groups (or silanol nests) as a result of incomplete condensation during the synthesis, thus reducing the catalytic performance.[34]

In this study, we focus on Ti-MWW, an isostructural analogue of the aluminosilicate MCM-22, as a potential candidate for cyclohexane oxidation.[35−37] Our choice is justified for several reasons. First, the Ti-MWW framework features two independent 10-ring channel networks (5.3 Å), one of which is connected to internal 12-ring supercages (7.1 × 18 Å) and side cups located at the external surface (7.0 Å).[38] Ti-MWW combines features of TS-1 and Ti-BEA, leading to a "hybrid" catalytic behavior between both zeolites: good activity in allyl alcohol and 1-hexene epoxidation, as found for TS-1,[39,40] and efficient epoxidation of cyclohexene using *t*-butyl hydroperoxide (TBHP), as found for Ti-BEA.[41] Second, Ti leaching during operation is low compared to Ti-beta and mesoporous titanosilicates. Third, Ti-MWW is more hydrophobic than Ti-BEA and Ti-MCM-41, the latter showing a high concentration of silanol groups and defect sites at the external surface. Note that the hydrophobicity of the parent Ti-MWW can be further increased by treatment with aqueous piperidine (PI) or hexamethylenimine (HMI) solutions, reducing by about 40% the number of internal silanol groups and defect sites (i.e., Al-free Ti-MWW).[42]

In light of the versatile oxidation properties offered by Ti-MWW, this zeolite might show potential as a deperoxidation catalyst for KA oil production. To this aim, we have chosen the oxidation of cyclohexane with TBHP as model reaction and compared the catalytic performance of Ti-MWW to that offered by TS-1, Ti-BEA, and Ti-MOR zeolites, all three considered as benchmark catalysts. The effect of the reaction temperature, time, catalyst amount, and catalytic stability of Ti-MWW was explored in detail. The location of the active sites was investigated by selective poisoning of the active sites. Electron paramagnetic resonance (EPR) experiments were combined with DFT calculations to study the reaction mechanism and gain insight into the nature of the active species during cyclohexane oxidation.

2. EXPERIMENTAL DETAILS AND COMPUTATIONAL METHODS

2.1. Chemicals. Four different Ti-containing zeolites with different effective channel sizes were selected to assess possible shape selectivity effects for cyclohexane oxidation: TS-1 (5.3 Å), Ti-MWW (5.3 Å, 7.0 Å), Ti-MOR (6.7 Å), and Ti-BEA (7.0 Å). Ti-MWW-1 (Si/Ti = 49) was obtained commercially from Zhejiang TWRD New Materials Co., Ltd., China, while Ti-MWW-2 (Si/Ti = 67), Ti-BEA (Si/Ti = 63), TS-1 (Si/Ti = 32), and Ti-MOR (Si/Ti = 84) zeolites were prepared on our premises following published recipes (see Supporting Information). Table 1 lists the textural properties and Ti/Si ratios (bulk and surface, noted respectively with 'b' and 's' subscripts) of the different samples.

Cyclohexane (>99%, Sinopharm), cyclohexanol (>97%, Sinopharm), cyclohexanone (>99.5%, Sinopharm), *t*-butyl hydroperoxide (TBHP, 70% in water, Aldrich), benzoquinone (BQ, >98%, Aldrich), tripropylamine (TPA, >98%, Fluka), triphenylamine (TPhA, 97%, Sinopharm), triphenylphosphine (TPP, >98.5%, Sinopharm), cyclohexene (>99%, Aladdin), cyclohexene oxide (>98%, Aladdin), 1-hexene (>99%, Aldrich), and 1,2-epoxyhexane (HO, 97%, Aldrich) were used as reagents. Cyclohexane containing TBHP (7.7 wt %) was prepared by extracting TBHP from water with cyclohexane (see Supporting Information). 1,2-Dichlorobenzene (DCB, >99%, Aldrich) was used as internal standard. Sodium thiosulfate ($Na_2S_2O_3$, 0.1 M, Sinopharm), potassium iodide (KI, 99.9%, Sinopharm), and potassium hydrogen carbonate ($KHCO_3$, 99.7%, Sinopharm) were used for the iodometric titration of TBHP.

2.2. Catalytic Oxidation of Cyclohexane Using *t*-Butyl Hydroperoxide (TBHP). A cyclohexane solution (4.0 g) containing TBHP (7.7 wt %, result from titration) was

dx.doi.org/10.1021/cs400757j | ACS Catal. 2014, 4, 53−62

introduced into a sealed tube under air together with the catalyst (0.1 g) on a preheated hot plate at 80 °C and subjected to mild stirring for 1 h. After cooling down to room temperature and centrifugation at 7200 rpm for 10 min, the reacted solution was removed from the tube and divided into two volumes for analysis. One volume was used for measuring the TBHP conversion after titration, while a given amount of 1,2-dichlorobenzene (DCB) was added to the second volume together with TPP to consume the unreacted TBHP for further analysis. The analyses were carried out in a GC (Agilent 7820A) equipped with a DB-WAX column and a flame ionization detector. Mass balances were accurate to within 5% in all the catalytic tests.

The KA selectivity was defined as the molar ratio between the produced KA compared to the converted TBHP by combining the titration and GC analytical methods, whereas the KA yield was defined as the molar ratio between the produced KA compared to the initial TBHP. The turnover number (TON) was computed as the molar ratio between the KA formed and the number of Ti sites after 1 h of reaction. Two TON numbers were defined (Table 1): TON_b referred to the total number of Ti sites (ICP values), and TON_s referred to the surface number of Ti sites (XPS values).

Some specific cyclohexane oxidation tests were carried out in the presence of TPA and TPhA for the Ti-MWW sample to unveil the location of Ti sites (i.e., over the inner 10-ring channels and 12-ring cavities or over the external 12-ring cups). Additional experiments were carried out by adding 1-hexene into the reaction mixture (cyclohexane/1-hexene = 6.3) to gain insight into the formation of nonradical species on the Ti sites.

Catalytic stability tests were carried out at 80 °C over 1 h at a solution/catalyst molar ratio of 40. After each run, the catalyst was washed with cyclohexane, dried at 100 °C, and calcined at 550 °C for 6 h before the next run.

2.3. Physical Characterization. Inductively Coupled Plasma Atomic Emission Spectroscopy (ICP-AES) was used to quantify the overall amount of Si and Ti in the different Ti-containing zeolites, as well as in the reaction system using a Thermo IRIS Intrepid II XSP atomic emission spectrometer. Before the measurements, the samples were dissolved using a HNO_3/HCl/HF solution.

The zeolite catalysts were characterized by X-ray powder diffraction (XRD) using a Rigaku D/MAX 2200 diffractometer (Cu Kα1 + 2 radiation).

UV−visible spectra were obtained on calcined zeolite powders using a JASCO V-670 (JASCO) spectrophotometer operating in diffuse reflectance mode to assess the nature of Ti species in the different samples. The measurements were performed in the wavelength range 190−500 nm. The spectroteflon standard from JASCO with 82% reflectivity was used as a reference.

The textural properties of the different zeolites were inspected by N_2 adsorption at 77.4 K using a Micrometrics Tristar II apparatus. Prior to the tests, the samples were degassed at 473 K under a vacuum (10^{-4} mbar) for 3 h. The BET specific surface was measured in the pressure range $0.05 < P/P_0 < 0.35$, while total pore volume was measured at $P/P_0 = 0.99$. The external surface was estimated using the *t*-plot method.

X-ray Photoelectron Spectra (XPS) were recorded on a Thermo ESCALAB 250 spectrometer with monochromatic Al Kα radiation ($h\nu$ = 1486.6 eV) to measure the surface Si/Ti molar ratio of the different samples.

Electron paramagnetic resonance (EPR) spectra were recorded at 118 K using a Bruker Elexsys e500 X-band spectrometer (9.42 GHz, 20.25 mW) with a standard cavity. The modulation amplitude and frequencies were 1 G and 100 kHz, respectively. The spectra were measured at 120 K on an aliquot of the reaction media containing both the solution and the catalyst after cyclohexane oxidation at 80 °C for 20 min. For the sake of comparison, EPR spectra were also measured after TBHP decomposition on the catalyst and after cyclohexene epoxidation with TBHP at 80 °C for 20 min. Before all the measurements, the reaction was quenched in a liquid N_2 bath (77.4 K).

2.4. DFT Simulations. We used a small cage-like cluster as model for Ti sites in Ti-MWW. The choice of this model is discussed in the Supporting Information. Density functional theory (DFT) calculations were performed with SPARTAN '10.1[43] for geometry optimization and energies, and ORCA 2.9.1[44] for the EPR *g* tensor. Optimization was carried out at the DFT (U)B3LYP/6-31G(d) level, while single point energies on the optimized structures were calculated at the (U)B3LYP/6-311+G(d,p) level using a Wachters all-electron basis set for Ti augmented by *f* functions.[45−47] The reported electronic energies (ΔE) were corrected for zero point energy (ZPE). ZPE, enthalpic, and entropic contributions were calculated at the (U)B3LYP/6-31G(d) level relying on harmonic frequencies scaled by a factor of 0.96. All structures were identified as minima on the potential energy surface by the absence of imaginary frequencies.

The influence of the solvent (cyclohexane) was checked using the SM8 and COSMO solvation models implemented in SPARTAN and ORCA, respectively. Since the effect on the structure and relative stability of the species was small (<10 kJ/mol difference), all here-reported values correspond to the gas phase. The EPR *g* tensor of radical species was calculated on optimized structures at the level used for single point energies using ORCA's default settings for the gauge origin (center of electronic charge). Using the larger EPR-III basis sets for O and accounting for solvent effects exerted no significant effect on the results.

3. RESULTS

3.1. XRD Patterns and Ti Distribution. Figure 1 shows the XRD patterns of the Ti-MWW framework after the synthesis, after calcination, and after four reaction cycles. The characteristic reflections around 3−7° in the as synthesized Ti-MWW sample reveal the formation of a layered structure along

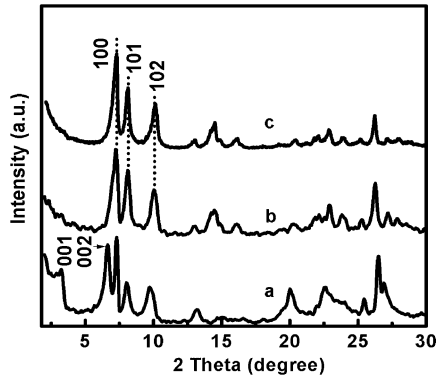

Figure 1. XRD patterns of Ti-MWW (Si/Ti_b = 49): (a) as-synthesized, (b) after calcination, and (c) after fourth use.

dx.doi.org/10.1021/cs400757j | ACS Catal. 2014, 4, 53−62

the *c* direction, while the other peaks are related to crystalline sheets parallel to *ab* planes. After calcination, (001) and (002) reflections disappeared, whereas (h00) and (hk0) reflections remained essentially unchanged. This observation can be ascribed to the formation of ordered linkages between sheets, this process occurring simultaneously with the loss of the lamellar structure upon calcination to result in the 3D MWW framework.

The Ti coordination environment of the two Ti-MWW samples after calcination was inspected by UV−visible spectroscopy (Figure 2). Only one band centered at 220 nm

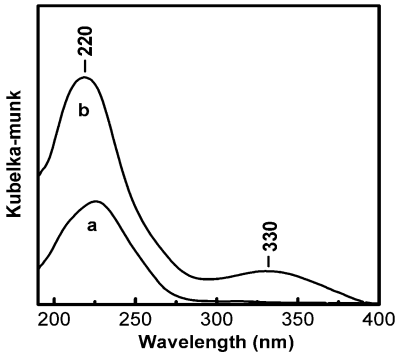

Figure 2. UV−visible spectra of (a) Ti-MWW (Si/Ti_b = 67) and (b) Ti-MWW (Si/Ti_b = 49) after calcination.

could be observed for Ti-MWW-2 (Si/Ti_b = 67), which can be attributed to a $Ti^{4+}O^{2-} \rightarrow Ti^{3+}O^{-}$ ligand-to-metal charge transfer and is indicative of tetrahedrally coordinated isolated Ti sites in the MWW framework.[48,49] However, when the Si/Ti_b ratio increased to 49 (i.e Ti-MWW-1), another band centered at 330 nm appeared, reflecting most likely the presence of ex-framework Ti species (e.g., octahedral Ti or anatase sites).[42] Similar UV−visible spectra were observed for TS-1 and Ti-BEA samples, while the Ti-MOR sample only presented apparently tetrahedral Ti sites (Supporting Information, Figure S1).

3.2. Screening of Ti-Zeolites. The four different Ti-containing zeolites prepared in this study were tested in the oxidation of cyclohexane with TBHP (7.7 wt % in cyclohexane) at 80 °C for 1.0 h. Among the different samples, Ti-MWW-1 (Si/Ti_b = 49) showed the highest selectivity and yield for KA oil with values of 90.1% and 9.64%, respectively (Table 1). A decrease of the bulk Ti content (i.e., Ti-MWW-2, Si/Ti_b = 67) promoted the TBHP conversion at the expense of a decline of the KA selectivity. We tentatively attribute such differences to a larger amount of silanol groups in the latter sample (i.e., more hydrophilic), promoting TBHP decomposition.

The turnover number for KA oil generation was calculated for the different zeolites as a function of the bulk Ti content (TON_b, Table 1). The TON_b increased in the order Ti-MOR (1.5) < TS-1 (2.1) < Ti-MWW-2 (7.7) < Ti-BEA (9.7) < Ti-MWW-1 (10.0). TS-1 showed much lower activity than Ti-BEA, which might be attributed to the small pore entrance (10-ring) of TS-1 channels, hindering the diffusion of cyclohexane to the Ti sites. In contrast, the two Ti-MWW samples with 12-ring side cups in addition to 10-ring channels showed an activity comparable to that of Ti-BEA. This observation suggests that in the case of Ti-MWW, the catalytic activity toward cyclohexane oxidation with TBHP is not only related to the effective pore size but also to the local environment of Ti. On the basis of these results, we further focused on the Ti-MWW-1 sample to investigate the effect of different reaction variables.

3.3. Catalytic Properties of Ti-MWW-1. *3.3.1. Effect of Temperature.* To explore the effect of temperature on the catalytic properties of Ti-MWW-1, a series of experiments were carried out in the range 80−140 °C. Table 2 collects the

Table 2. Effect of Reaction Temperature on Cyclohexane Oxidation over Ti-MWW[a]

T (°C)	cyclohexane conv. %[b]	TBHP conv. %	KA sel. %	KA yield %	A/K	TON_b[c]
80	0.8	11.7	83.7	9.8	6.4	8.4
100	1.5	24.8	75.9	18.8	3.9	16.3
120	1.9	65.8	36.2	23.8	2.4	21.7
140	3.0	96.5	39.8	38.4	2.4	33.1

[a]Reaction conditions: 80 °C, 1.5 h, 0.10 g catalyst, 4 g of cyclohexane containing 7.7 wt % TBHP. [b]Cyclohexane conversion was calculated based on molar percentage of converted KA oil to original cyclohexane. [c]TON_b = KA yield (mol)/total Ti site (mol) in Ti-MWW.

cyclohexane and TBHP conversion, and KA selectivity and yield. Both TBHP conversion and KA yield increased with the reaction temperature, while the KA selectivity and A/K molar ratio decreased. At 140 °C, TBHP was almost fully consumed, the KA yield reaching a maximum value ca. 40%, but at the expense of a much lower KA selectivity (83.7% at 80 °C compared to 39.8% at 140 °C). The decrease of the KA selectivity was probably caused by the self-decomposition of TBHP on Ti and silanol sites, this process being promoted by temperature.[50]

3.3.2. Effect of the Reaction Time. The effect of the reaction time was surveyed from 1 to 24 h (Table 3). Both cyclohexane

Table 3. Effect of Reaction Time on Cyclohexane Oxidation over Ti-MWW[a]

time (h)	cyclohexane conv. %	TBHP conv. %	KA sel. %	KA yield %	A/K
1.0	0.8	10.7	90.1	9.6	8.4
1.5	0.8	11.7	83.7	9.8	7.4
3.0	0.9	22.3	53.5	11.9	5.3
24	1.2	43.0	36.9	15.9	2.6

[a]Reaction conditions: 80 °C, 0.10 g catalyst, 4 g of cyclohexane containing 7.7 wt % TBHP.

conversion and KA yield increased slightly with time, while KA selectivity decreased from an initial value of ca. 90.1% after 1 h to 36.9% after 24 h. These results reflect a higher self-decomposition of TBHP with the reaction time, cyclohexane oxidation mainly occurring during the first 1 h of reaction. In this period, only cyclohexanol was produced in the very beginning of the reaction, whereas cyclohexanone was generated after 20 min.

3.3.3. Effect of the Catalyst Weight. We also explored the effect of the catalyst weight on the reaction (Table 4). The KA yield increased with the catalyst weight in the range 0.05−0.2 g, indicating a higher specific activity of Ti moieties mostly ascribed to a higher TBHP conversion. In contrast, both KA selectivity and A/K ratio were found to decrease with the catalyst amount, probably due to a longer residence time of the reactants on Ti sites.

dx.doi.org/10.1021/cs400757j | ACS Catal. 2014, 4, 53−62

Table 4. Effect of Catalyst Amount on Cyclohexane Oxidation over Ti-MWW[a]

amount (g)	Ti/TBHP mol %	TBHP conv. %	KA sel. %	KA yield %	A/K
0.05	0.63	4.7	94.3	4.4	10.3
0.10	1.26	10.7	90.1	9.6	8.4
0.20	2.52	22.5	60.7	13.7	3.6
0.30	3.78	22.1	49.4	10.9	3.3

[a]Reaction conditions: 80 °C, 1.0 h, 4 g of cyclohexane with 7.7 wt % TBHP.

3.3.4. Catalytic Stability. The catalytic stability of the Ti-MWW-1 sample was also investigated after 1−4 runs at 80 °C for 1 h using a catalyst weight of 0.1 g and 4 g of cyclohexane containing 7.7 wt % TBHP. The catalyst was dried at 100 °C and calcined at 550 °C for 6 h before the next run. The catalyst showed a stable performance in terms of TBHP conversion and KA selectivity (Figure 3), suggesting no deactivation by either

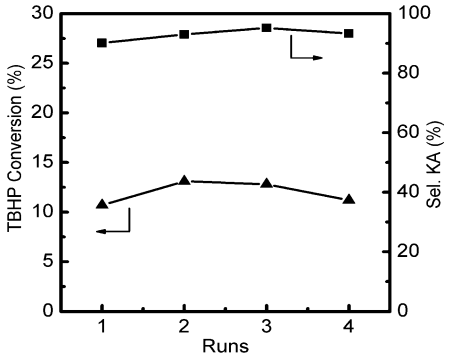

Figure 3. Catalytic results of Ti-MWW-1 in the oxidation of cyclohexane for four repeated consecutive runs with regeneration.

pore blockage or potential Ti leaching during operation. This observation also suggests an unmodified distribution of active intermediate species on the Ti sites during operation.

To confirm the integrity of the sample after reaction, the Ti-MWW-1 sample was characterized by XRD and ICP before reaction and after the fifth run. From the ICP analyses, the Ti content kept almost unchanged after recycling (Table 1, first row), while no Ti was detected in the solution. These results support the behavior of Ti-MWW as a truly heterogeneous catalyst during cyclohexane oxidation. Reused Ti-MWW-1 showed no detectable change in the XRD pattern compared to the calcined samples (Figure 1), confirming the stability of the Ti-MWW framework during reaction.

3.3.5. Location of the Active Ti Sites in Ti-MWW: Position-Selective Poisoning. Given the promising results reported above on cyclohexane oxidation over Ti-MWW, we decided to carry out some additional experiments and characterization tests to gain insight into the reaction mechanism. On the guidance of a previous study,[41] we first used position-selective poisoning reagents to unveil the position of the active Ti sites (i.e., in the inner 10-ring channels and 12-ring supercages, or near 12-ring side cups located at the external surface of the MWW framework). To address this issue, we selected two molecular probes: (1) tripropylamine (TPA), which is expected to enter both the inner 10-ring channels and 12-ring supercages and consequently poison all the Ti sites, and (2) the bulky triphenylamine (TPhA), which is too large to enter the 10-ring channels and thus should selectively poison the active Ti sites located at the external 12-ring cups. In both cases, after reaction, the KA yield showed a dramatic yet comparable decrease (Table 5), suggesting that most of the Ti sites

Table 5. Position-Selective Poisoning Reagents (PR) over Ti-MWW for Cyclohexane Oxidation before and after Introduction of 1-Hexene (in Parentheses)[a]

PR	PR/Ti	TBHP conv. %	sel. KA %	KA yield (mmol)	HO[b] yield (mmol)
none	0	10.7	90.1	0.33 (0.05)	−(4.90)
TPA	17	0.2	1.3	<0.01 (<0.01)	−(0.02)
TPhA	17	0.1	5.0	0.01 (<0.01)	−(0.18)

[a]Reaction conditions: 80 °C, 1.0 h, 0.10 g catalyst, 4 g cyclohexane with 7.7 wt % TBHP. The experiments in the presence of 1-hexene were performed for a cyclohexane/1-hexene molar ratio of 6.3. [b]1,2-Epoxyhexane.

participating in the oxidation of cyclohexane with TBHP are located within the 12-ring cups at the external surface of the Ti-MWW particles.

Considering then that cyclohexane oxidation with TBHP over Ti-MWW proceeds mainly on 12-ring cups (Scheme 1),

Scheme 1. Graphic Illustration of KA Oil Formation on 12-Ring Side Cups of Ti-MWW

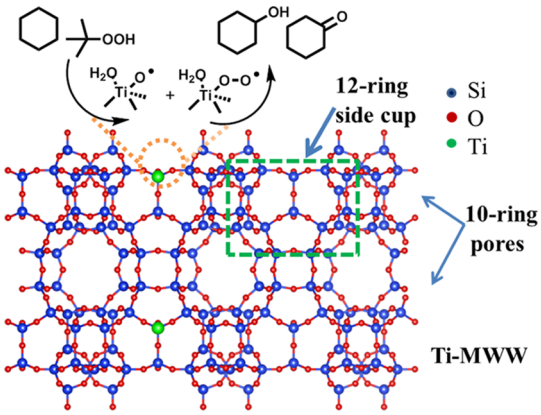

we computed the turnover number of the reaction only relying on the active external Ti sites measured by XPS (i.e., TON_s, Table 1). A similar approach was considered for TS-1, while for Ti-Beta and Ti-MOR, the total Ti loading (measured by ICP) was considered since in the latter case the inner Ti sites are also expected to be active. Among the different zeolites, the Ti-MWW-1 sample showed the highest TON_s values. We also computed the TON_s for the Ti-MWW-2 sample (Si/Ti_b = 67), displaying a value similar to that obtained for Ti-MWW-1 (Si/Ti_b = 49; Table 1). All these results suggest that the higher activity of Ti-MWW can be attributed to its unique framework including 12-ring cups and also to an improved accessibility of the Ti sites compared to the other tested zeolites.

3.3.6. Competition between Cyclohexane Oxidation and 1-Hexene Epoxidation. When the catalytic test was carried out with a mixture of 1-hexene and cyclohexane (cyclohexane/1-hexene = 6.3), the production of KA oil was almost shut down. The main product was now 1,2-epoxyhexane (HO) originating from 1-hexene epoxidation (Table 5, first row, value in parentheses). This finding strongly suggests that 1-hexene and cyclohexane compete for the same Ti centers.

dx.doi.org/10.1021/cs400757j | ACS Catal. 2014, 4, 53−62

To further confirm this hypothesis, we repeated the same experiment in the presence of the above stated position-poisoning agents (i.e., TPA and TPhA). Both reaction products, KA oil and HO, were found to largely decrease after TPA and TPhA addition (Table 5, third row, value in parentheses), even if a small yet non-negligible amount of HO was still produced. This result is to be compared with 1-hexene epoxidation with H_2O_2 over Ti-MWW and TS-1, where the reaction was strongly inhibited by TPA, whereas TPhA only reduced slightly the activity.[41] In that case, the active Ti sites are believed to reside in the 10-ring channels. However, TBHP is much bulkier than H_2O_2 and thus is not expected to diffuse into the 10-ring channels, which could explain why in our case both poisoning agents exerted a similar effect.

Overall, we can conclude that the same sites on 12-ring cups are involved in both alkane oxidation and alkene epoxidation. The (quasi)-absence of reaction in the 10-ring channels is in both cases most probably due to the intrinsic bulkiness of TBHP, preventing the access to the internal active sites.

3.3.7. EPR Investigation. According to previous studies on homogeneous and heterogeneous catalysts,[50,51] cyclohexane oxidation by TBHP appears to proceed via a radical chain mechanism. However, according to alkene epoxidation studies over titanosilicates (most often TS-1),[52−54] *in situ* IR and UV Raman tests,[55−58] and DFT calculations,[59−62] the formation of nonradical hydroperoxo/peroxo-titanium intermediates has been suggested when using either H_2O_2 or TBHP as an oxidant. In the case of TBHP, the formation of Ti(OOtBu) species has been established in previous reports by a combination of EXAFS (Extended X-ray Absorption Fine Structure)[63] and DFT calculations.[64,65] These species can be seen as analogues of Ti(OOH) species formed upon reaction with H_2O_2.

To provide direct evidence for the presence of radical species, a series of rationally designed electron paramagnetic resonance (EPR) experiments was performed. Considering that the reactants, reaction products, and Ti(IV) moieties on Ti-MWW are all diamagnetic and accordingly EPR-silent, any EPR signal would indicate the presence of species with unpaired electrons. To this aim, after running the reaction at 80 °C for 20 min, an aliquot of the reaction medium containing both the solution and the catalyst was transferred to an EPR tube. The reaction was quenched in a liquid N_2 bath (77.4 K), and the EPR spectrum was measured at 120 K. As a general rule, an EPR-active species can be characterized by three g values corresponding to the trace of the g tensor. These values can differ for asymmetric species (*vide infra*).

Figure 4 shows the experimental EPR spectra measured for the Ti-MWW + TBHP + cyclohexane system after 20 min of reaction at 80 °C (spectrum A) and for Ti-MWW + TBHP + acetonitrile under analogous reaction conditions, *i.e., without* cyclohexane (spectrum B). To guide the assignment of g values to a given species, it is important to pay attention to the line width of each individual peak and its relative intensity. Keeping this idea in mind, the signals in spectrum A were attributed to two different species with g_{xx}^{1}, = 2.0028, g_{yy}^{1} = 2.0107, g_{zz}^{1} = 2.026, and g_{xx}^{2} = 2.0046, g_{yy}^{2} = 2.0138, g_{zz}^{2} = 2.049, respectively. Finally, a very small signal at g = 2.0000 is likely due to the cavity or residual organic radicals and will not be discussed further. In contrast, the direct reaction of Ti-MWW with TBHP in acetonitrile produced a broad and thus markedly different EPR signal with $g_{xx}^{1'}$ = 2.0028, $g_{yy}^{1'}$ = 2.0107, and $g_{zz}^{1'}$ = 2.020 (spectrum B). A second species was apparently observed with

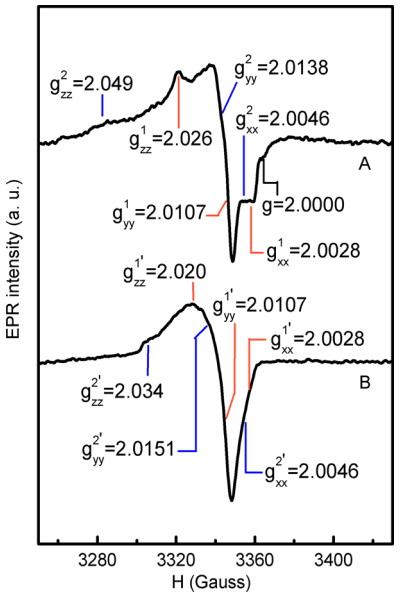

Figure 4. EPR spectra at 120 K of the reaction mixture after 20 min, i.e. Ti-MWW + cyclohexane + TBHP (A) and Ti-MWW + acetonitrile + TBHP (B). g refers to the top spectrum, while g′ refers to the bottom spectrum. Color code: blue for species 1 and orange for species 2 in Table 7.

$g_{xx}^{2'}$ = 2.0046, $g_{yy}^{2'}$ = 2.0151, and $g_{zz}^{2'}$ = 2.034. More details about the nature of both species and their potential formation pathways are provided below.

Additional experiments were carried out to check whether the reactants and the catalyst (i.e., TBHP, Ti-MWW + cyclohexane) could produce an EPR signal. In all cases (not shown), the different systems were inactive in EPR, even if dissolved oxygen (paramagnetic) was present in the samples. Finally, cyclohexene oxidation over Ti-MWW using TBHP was also monitored by EPR under the same reaction conditions. As expected for a nonradical reaction, no EPR signal was observed, while the yield of cyclohexene oxide kept similar to the value measured without BQ (Table 6), confirming the consistency of the EPR spectra for cyclohexane oxidation.

Table 6. Effect of Radical Scavengers[a]

reactant	system	BQ/TBHP	BQ/Ti	KA yield (mmol)	CO[b] yield (mmol)
cyclohexane	TiMWW	0	0	0.33	–
	TiMWW +BQ	0.193	15.7	0.02	–
cyclohexene	TiMWW	0	0	–	3.35
	TiMWW +BQ	0.193	15.7	–	3.18

[a]Reaction conditions: 80 °C, 1.0 h, 0.10 g catalyst, 4 g of cyclohexane/cyclohexene containing 7.7 wt % TBHP. BQ: p-benzoquinone. [b]CO: cyclohexene oxide.

4. DISCUSSION

From the experimental results reported above, as far as the reaction mechanism is concerned, two main conclusions emerge: (i) cyclohexane oxidation takes place on Ti sites mainly located in the external 12-ring cups, and (ii) the reaction proceeds through radical intermediates. The epoxidation of 1-hexene, which was studied for comparison, takes place on the

dx.doi.org/10.1021/cs400757j | ACS Catal. 2014, 4, 53−62

Scheme 2. (i) Formation of Ti-(η^2-OOtBu)(H_2O) and (ii−iv) Formation of Potential Radical Intermediates via Uni- and Bimolecular Cleavage of Ti-η^1(OOtBu)(H_2O)[a]

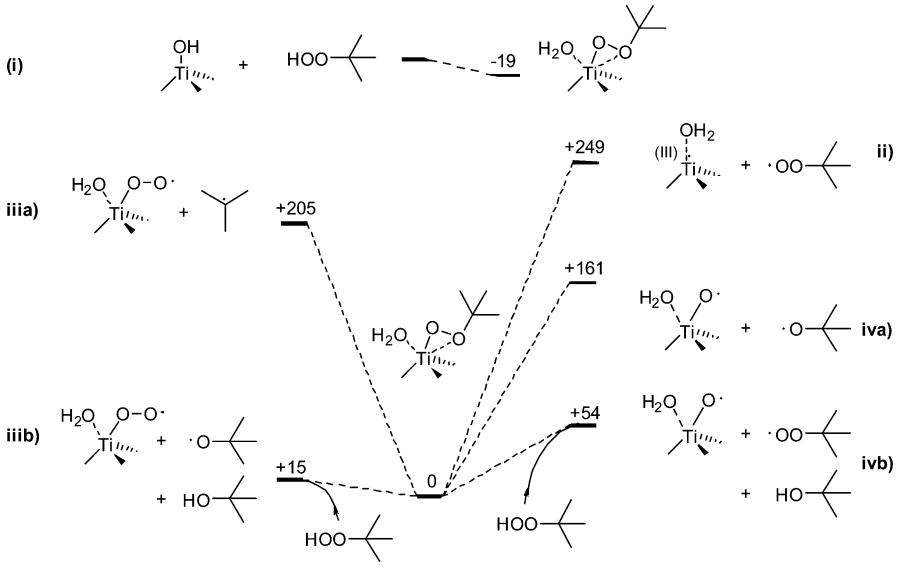

[a]Energies (ΔE, kJ/mol) are given relative to this species (and tBuOOH in the case of bimolecular pathways). The full structures are reported in the Supporting Information.

same external Ti sites, but it does not involve radical intermediates. Accordingly, radical species appear to coexist with nonradical intermediates on Ti sites.

Apart from the above-mentioned implication of radical species, little is known about the mechanism of alkane oxidation in Ti-containing zeolites. To gain insight into the reaction mechanism and assist the assignement of the EPR spectra, we investigated the stability of potential radical species and calculated their EPR-spectroscopic signature by DFT. In particular, the striking differences between the EPR spectra obtained in the presence and in the absence of cyclohexane triggered such investigation.

4.1. Formation of Ti-Centered Radical Species: DFT Calculations. We chose $(SiO)_3Ti(\eta^2\text{-}OOtBu)(H_2O)$ as the starting point for the study of potential radical intermediates (Scheme 2, reaction i). The formation of this species is discussed in the Supporting Information (Figure S2), since our results are very similar to literature data.[61] Ti is 5-fold coordinated in the starting structure. Such extension of the coordination sphere by water (which is formed by the reaction of TiOH with tBuOOH) is generally accepted, and both 6-fold and more recently 5-fold coordination have been suggested.[66] Note that 6-fold coordination does not significantly affect the trends outlined here (see Scheme S2 and Figure S2).

The homolytic fragmentation of Ti(OOtBu) can yield in principle three species: (i) Ti(III)•, (ii) Ti(IV)-OO• (peroxyl, Figure 5a), and (iii) Ti(IV)-O• (oxyl, *Figure* 5b). Ti(III)• species on Ti-containing zeolites have indeed only been observed in rather reductive media in the presence of H_2, CO,[67,68] or hydrides.[69] The occurrence of peroxyl radicals in Ti-containing silicalites in contact with H_2O_2 or organic peroxides has been established by EPR.[70−74] Ti(IV)-O• (oxyl) species, although already proposed by Clerici in the past decade,[75] have almost never been considered. Indeed, only recently was its formation in the presence of H_2O_2 investigated by DFT calculations.[42] This is somewhat surprising, since Ti(OOR) can be seen as an analogue of HOOR (R = H, alkyl),

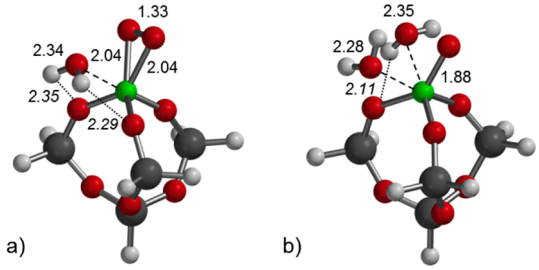

Figure 5. Representative radical species as obtained from DFT calculations: (a) Ti(OO•)H_2O and (b) Ti(O•)$(H_2O)_2$. Distances are given in Å. Italics are used for H-bonding distances. Nomenclature: O, red ball; H, light gray; Ti, green ball; Si, gray ball.

and breaking the O−O bond is by far the easiest source of radicals from both H_2O_2 and tBuOOH (Scheme S1).

Ti(III)• can be formed by homolytic splitting of the Ti−O bond, yielding a tBuOO• radical (Scheme 2, reaction ii). However, this process is highly unfavorable (ΔE = +249 kJ/mol), even when fully stabilized by water (see Supporting Information).

Ti(IV)-OO• (peroxyl) can be formed by the loss of a *t*-butyl radical (Scheme 2, reaction iiia), but this process is likewise unfavorable (ΔE = +205 kJ/mol). In a similar fashion, Ti(IV)-O• can be formed by the loss of a tBuO• radical (Scheme 2, reaction iva). As expected from the weakness of the O−O bond, this process is more favorable, but still high in energy (ΔE = +161 kJ/mol). Since the fragmentations are entropically favored, accounting for such contribution provides more favorable reactions (ΔG_{298} is on average 60 kJ/mol lower than ΔE).[76] Still, the direct fragmentations presented so far cannot probably account for the species observed in the experiments.

However, as suggested by Clerici,[77] and recently calculated for H_2O_2,[64] bimolecular pathways implying the participation of a second peroxide molecule could explain the formation of the Ti(IV)-O• (oxyl) species. Indeed, such a reaction, yielding a

dx.doi.org/10.1021/cs400757j | ACS Catal. 2014, 4, 53−62

Table 7. Comparison of EPR g Values of Different Ti Species from Experiment and DFT Calculations

species[a]		EPR g tensor[b] g_{xx}	g_{yy}	g_{zz}	g_{iso}	source
Ti-peroxyl Ti(IV)-OO•	species 1	2.0033	2.0095	2.0269	2.0132	Exp, TS-1 + H_2O_2 [70]
	species 1′	2.0033	2.0095	2.0234	2.0120	
	species 1	2.0023	2.0090	2.0280	2.0131	Exp, TS-1 + H_2O_2 [72]
	species 1′			2.0200		
	species 1	2.0023	2.0090	2.0266	2.0126	Exp, TS-1 + H_2O_2 [73]
	species 1′	2.0023	2.0090	2.0238	2.0117	
	Ti(OO•)	2.0027	2.0096	2.0280	2.0134	DFT, this study
	Ti(OO•)(H_2O)	2.0028	2.0096	2.0266	2.0130	
	Ti(OO•)(H_2O)$_2$	2.0031	2.0094	2.0243	2.0123	
	average	2.0029	2.0095	2.0263	2.0129	
	species 1-A	**2.0028**	**2.0107**	**2.026**[c]	**2.0132**	**Exp, this study**
	species 1-B	**2.0028**	**2.0107**	**2.020**[c]		
Ti-oxyl Ti(IV)-O•	Ti(O•)	2.0046	2.0143	2.0713	2.0301	DFT, this study
	Ti(O•)(H_2O)	2.0042	2.0131	2.0309	2.0161	
	Ti(O•)(H_2O)$_2$	2.0045	2.0151	2.0426	2.0207	
	Ti(O•)(H_2O)$_3$	2.0047	2.0103	2.0246	2.0132	
	average	2.0045	2.0132	2.0424	2.0200	
	species 2-A	**2.0046**	**2.0138**	**2.049**[c]	**2.0225**	**Exp, this study**
	species 2-B	**2.004**	**2.015**	**2.034**[c]		

[a]Species 1 and 1′ differ one another due to solvent effects. [b]g value accuracy estimated from field values known at ±0.5 G, i.e., ± 0.003, for convenience, x, y, and z componants are assigned arbitrarily from the smallest to the highest g values, i.e., from right to left in Figure 4. [c]Lower accuracy on g of ±0.001 due to broad line width.

tBuOO• radical and tBuOH (as experimentally observed), is much lower in energy (reaction ivb in Scheme 2, ΔE = +54 kJ/mol) and even favorable in terms of Gibbs free energy (ΔG_{298} = −8 kJ/mol). The reaction (ΔE) energy is close to the value calculated for Ti(IV)-O• formation starting from Ti(OOH) and H_2O_2 (+40 kJ/mol),[64] being also consistent with the similar O−O bond dissociation energy for both peroxides (Scheme S1). This suggests that Ti(IV)-O• radical species are thermodynamically accessible. Note also that the reaction was carried out experimentally at 80 °C, favoring even more the thermodynamics of the process. Along these lines, we can also propose a bimolecular dissociation to yield Ti(IV)-OO• (peroxyl) species. In stark contrast to the unimolecular fragmentation, this process is favorable (ΔE = +15 kJ/mol, ΔG_{298} = −63 kJ/mol). In summary, bimolecular pathways can rationalize from a thermodynamic viewpoint the formation of Ti(IV)-OO• and Ti(IV)-O• species.

4.2. Interpretation of the EPR Spectra. The calculated EPR g tensor of the above-discussed energetically accessible radical species is reported together with our experimental and literature data in Table 7. Additional peak data obtained after deconvolution can be found in the Supporting Information (Figure S4, Table S2). Since hydration affects the structure of Ti sites, we expect an effect on the g-tensor.[78] Therefore, we modeled different states of hydration (SI, Figure S3). Indeed, previous experimental studies on the TS-1/H_2O_2/H_2O system reported in most cases the formation of two different Ti-peroxyl radicals, Ti(IV)-OO•, that can be a priori attributed to three different species: (1) species a with different number of coordinated water molecules,[70] (2) species formed in framework and ex-framework Ti moieties,[71] and (3) species formed in tetrapodal (external) or tripodal (internal) Ti sites.[72−74] Furthermore, as pointed out by Wells et al.,[65] we do not exclude a possible stabilization by surface silanol groups (defects). In our case, the experiments carried out in the sole presence of TBHP were subjected *per se* to a much higher hydration level than those in the presence of cyclohexane, since in the former experiments TBHP was highly diluted in water (ca. 30 wt %) to ensure its stability. In the second case, even if water was present at trace level after TBHP extraction with cyclohexane and could also be generated during cyclohexane oxidation, the hydration level is expected to be much lower due to the low reaction time used (20 min).

The EPR signals referred to as species 1-A and species 1-B in the Ti-MWW + TBHP + cyclohexane and Ti-MWW + TBHP + acetonitrile systems (Figure 4, spectra A and B, respectively) show very similar g^1 and $g^{1'}$ values within the limits of the experimental error (Table 7), even if the Ti centers in the second system are expected to show a higher degree of hydration. This observation matches the trends predicted by DFT for Ti(IV)-OO• species, the corresponding g values being confined in a very narrow range (average over all hydration states: g_{xx} = 2.0029, g_{yy} = 2.0095, g_{zz} = 2.0263 in Table 7) and essentially insensitive to hydration, except for g_{zz}, which varies slightly. Relying on these calculations and on the experimental data from the literature (species 1 and 1′ in Table 7), species 1-A and species 1-B can both be assigned to Ti(IV)-OO•, but their state of hydration is difficult to ascertain, since the effect of hydration is weak.

The EPR spectrum of the reaction mixture (Figure 4, spectrum A) shows an additional signal (species 2-A) which cannot be attributed to Ti(IV)-OO• or any species reported so far in the literature. However, we find a very good agreement with the g values calculated for Ti(IV)-O•. All principal values calculated for Ti(IV)-O• are significantly higher than those found for Ti(IV)-OO• (average over all hydration states: g_{xx} = 2.0045, g_{yy} = 2.0132, g_{zz} = 2.0424). While g_{xx} is almost not affected by hydration and g_{yy} varies only slightly, g_{zz} is strongly affected by hydration, much more than for Ti(IV)-OO•. In light of these results, species 2-A and species 2-B might be tentatively assigned to different hydrated forms of Ti(IV)-O•. In spectrum B, it is more difficult to argue for the presence of

dx.doi.org/10.1021/cs400757j | ACS Catal. 2014, 4, 53−62

Ti(IV)−O$^{\bullet}$ species, most likely due to a masking effect of water and thus hydration. Indeed, the predicted g values for Ti(IV)-OO$^{\bullet}$ and Ti(IV)-O$^{\bullet}$, more specifically g_{yy} and g_{zz}, are relatively close when 2 or more water molecules are coordinated to the Ti center (Table 7, Figure 5). This effect of hydration might explain why the Ti(IV)-O$^{\bullet}$ species is hardly detectable in spectrum B in Figure 4 and also in analogous spectra published in the literature, typically measured under aqueous or strongly hydrated conditions.

Note finally that Ti(III)$^{\bullet}$ is predicted at g values (<2.0000) not compatible with the experiment (Table S1), which is consistent with its unfavorable formation.

5. CONCLUSIONS

We have shown that Ti-MWW zeolite exhibits a much higher selectivity to KA oil during the oxidation of cyclohexane with TBHP than other titanium zeolites such as TS-1, Ti-Beta, and Ti-MOR. The higher performance of Ti-MWW was attributed to its unique structure providing accessible Ti sites on external 12-ring cups. Unlike the reaction time and the catalyst weight, the temperature exerted a remarkable effect on the catalytic performance. Ti-MWW exhibited a high stability in the reaction and could be reused for at least four runs keeping a similar activity and with no detectable Ti leaching.

In the simultaneous presence of alkenes, competition between radical (alkane oxidation) and nonradical (alkene epoxidation) mechanisms took place, suggesting that both reactions share the same precursor at the active site, presumably Ti-OOtBu species.

In situ EPR experiments combined with DFT calculations suggested the formation of at least two Ti-centered radical species in our reaction system. One of the signals could be unambiguously assigned to peroxyl species, Ti(IV)-OO$^{\bullet}$, as frequently reported in the literature. In contrast, the other signal was not compatible with such species but provided instead an excellent match with the EPR g tensor values calculated for oxyl radicals, Ti(IV)-O$^{\bullet}$. Although oxyl radicals have been proposed as active centers for alkane oxidation, to the best of our knowledge they have not been observed so far. However, opposed to the published literature, our spectra have been recorded under anhydrous conditions, and indeed our calculations suggest that strong hydration makes the distinction between Ti(IV)-OO$^{\bullet}$ and Ti(IV)-O$^{\bullet}$ difficult. Both radical intermediates might be generated via bimolecular pathways as a reminiscence of a homolytic O−H and O−O cleavage, respectively.

We believe that the high catalytic performance of our system should motivate further development of Ti-based oxidation catalysts. In addition, the possible observation of Ti(IV)-O$^{\bullet}$ species opens up new mechanistic perspectives for alkane oxidation, which, in contrast to alkene epoxidation, is still poorly understood. Further investigation of the presence of Ti(IV)-O$^{\bullet}$ in other Ti-containing zeolites is under study.

■ ASSOCIATED CONTENT

Supporting Information

UV−visible spectroscopy of Ti-MOR, Ti-Beta, and TS-1 zeolites. Structures of the species involved in the formation of Ti(OOtBu). Structures of the species originating from fragmentation of Ti(OOtBu). Experimental (blue) and simulated (green) spectrum A. Bond dissociation enthalpies (>H_{298}, kcal/mol) calculated for H_2O_2 and tBuOOH at the G3(MP2) level of theory with the Spartan '10 software. Formation of Ti-η^1(OOtBu)$(H_2O)_n$ and potential radical intermediates via uni- and bimolecular cleavage of Ti-η^1(OOtBu)$(H_2O)_n$. Calculated principal values of the EPR g tensor for Ti(III) species. EPR g values obtained from deconvolution of spectrum A. Additional experimental details and choice of the model for DFT calculations. This material is available free of charge via the Internet at http://pubs.acs.org.

■ AUTHOR INFORMATION

Corresponding Authors

*E-mail: marc.pera-titus-ext@solvay.com.

*E-mail: pwu@chem.ecnu.edu.cn.

Notes

The authors declare no competing financial interest.

■ ACKNOWLEDGMENTS

W.-J.Z thanks China Postdoctoral Science Foundation (grants 2013M541493). P.W. gratefully acknowledges NSFC (grants 20925310, U1162102, 21373089) and the Ph.D. Program Foundation of the Ministry of Education of China (grant 2012007613000).

■ REFERENCES

(1) Ulrich, H. *Raw Materials for Industrial Polymers*; Hanser Publishers: Munich, Germany, 1988.
(2) Castellan, A.; Bart, J. C. J.; Cavallaro, S. *Catal. Today* **1991**, *9*, 237.
(3) Suresh, A. K.; Sharma, M. M.; Sridhar, T. *Ind. Eng. Chem. Res.* **2000**, *39*, 3958.
(4) Schuchardt, U.; Cardoso, D.; Sercheli, R.; Pereira, R.; da Cruz, R. S.; Guerreiro, M. C.; Mandelli, D.; Spinacé, E. V.; Pires, E. L. *Appl. Catal., A* **2001**, *211*, 1.
(5) Zhao, R.; Ji, D.; Lv, G.; Qian, G.; Yan, L.; Wang, X.; Suo, J. *Chem. Commun.* **2004**, 904.
(6) Zhan, B. Z.; White, M. A.; Pincock, J. A.; Robertson, K. N.; Cameron, T. S.; Sham, T. K. *Can. J. Chem.* **2003**, *81*, 764.
(7) Saint-Arroman, R. P.; Basset, J.-M.; Lefebvre, F.; Didillon, B. *Appl. Catal., A* **2005**, *290*, 181.
(8) Breynaert, E.; Hermans, I.; Lambie, B.; Maes, G.; Peeters, J.; Maes, A.; Jacobs, P. *Angew. Chem., Int. Ed.* **2006**, *45*, 7584.
(9) Chen, J. D.; Dakka, J.; Sheldon, R. A. *Appl. Catal. A: General* **1994**, *108*, L1.
(10) Armengol, E.; Corma, A.; Fornés, V.; Garcia, H.; Primo, J. *Appl. Catal., A* **1999**, *181*, 305.
(11) Selvam, P.; Dapurkar, S. E. *J. Catal.* **2005**, *229*, 64 q.
(12) Prabhu, A.; Kumaresan, L.; Palanichamy, M.; Murugesan, V. *Appl. Catal., A* **2010**, *374*, 11.
(13) Moliner, M.; Corma, A. *Microporous Mesoporous Mater.* **2013**, in press.
(14) Notari, B. *Adv. Catal.* **1996**, *41*, 253.
(15) Camblor, M. A.; Corma, A.; Pérez-Pariente, J. *Zeolites* **1993**, *13*, 82.
(16) Corma, A.; Camblor, M. A.; Esteve, P.; Martinez, A.; Pérez-Pariente, J. *J. Catal.* **1994**, *145*, 151.
(17) Corma, A.; Esteve, P.; Martinez, A. *J. Catal.* **1996**, *161*, 11.
(18) Sasidharan, M.; Wu, P.; Tatsumi, T. *J. Catal.* **2002**, *205*, 332.
(19) Tuel, A. *Zeolites* **1995**, *15*, 236.
(20) Moliner, M.; Serna, P.; Cantin, Á.; Sastre, G.; Díaz-Cabanas, M. J.; Corma, A. J. *Phys. Chem. C* **2008**, *112*, 19547.
(21) Wu, P.; Komatsu, T.; Yashima, T. *J. Phys. Chem.* **1996**, *100*, 10316.
(22) Davies, L. J.; McMorn, P.; Bethell, D.; Bulman Page, P. C.; King, F.; Hancock, F. E.; Hutchings, G. J. *J. Mol. Catal. A: Chem.* **2001**, *165*, 243.
(23) Igarashi, N.; Kidani, S.; Ahemaito, R.; Hashimoto, K.; Tatsumi, T. *Microporous Mesoporous Mater.* **2005**, *81*, 97.

(24) Hereijgers, B. P. C.; Weckhuysen, B. M. *J. Catal.* **2010**, *270*, 16.
(25) Kumar, A.; Srinivas, D. *Catal. Today* **2012**, *198*, 59.
(26) Wang, J.; Xu, L.; Zhang, K.; Peng, H.; Wu, H.; Jiang, J.-G.; Liu, Y.; Wu, P. *J. Catal.* **2012**, *288*, 16.
(27) Reichinger, M.; Schmidt, W.; van den Berg, M. W. E.; Aerts, A.; Martens, J. A.; Kirschhock, C. E. A.; Gies, H.; Grünert, W. *J. Catal.* **2010**, *269*, 367.
(28) Sanz, R.; Serrano, D. P.; Pizarro, P.; Moreno, I. *Chem. Eng. J.* **2011**, *171*, 1428.
(29) Zhou, J.; Hua, Z.; Cui, X.; Ye, Z.; Cui, F.; Shi, J. *Chem. Commun.* **2010**, *46*, 4994. Wang, W.; Li, G.; Li, W.; Liu, L. *Chem. Commun.* **2011**, *47*, 3529.
(30) Tamura, M.; Chaikittisilp, W.; Yokoi, T.; Okubo, T. *Microporous Mesoporous Mater.* **2008**, *112*, 202.
(31) Maschmeyer, T.; Rey, F.; Sankar, G.; Thomas, J. M. *Nature* **1995**, *387*, 159.
(32) Kraushaar, B.; van Hooff, J. H. C. *Catal. Lett.* **1998**, *1*, 81.
(33) Krijnen, S.; Sanchez, P.; Jakobs, B. T. F.; van Hoof, J. H. C. *Microporous Mesoporous Mater.* **1999**, *31*, 163.
(34) Park, S.; Cho, K. M.; Youn, M. H.; Seo, J. G.; Jung, J. C.; Baeck, S.-H.; Kim, T. J.; Chung, Y.-M.; Oh, S.-H.; Song, I. K. *Catal. Commun.* **2008**, *9*, 2485.
(35) Wu, P.; Tatsumi, T. *Chem. Commun.* **2001**, 897.
(36) Wu, P.; Tatsumi, T.; Komatsu, T.; Yashima, T. *Chem. Lett.* **2000**, 774.
(37) Wu, P.; Tatsumi, T.; Komatsu, T.; Yashima, T. *J. Phys. Chem. B* **2001**, *105*, 2897.
(38) Leonowicz, M. E.; Lawton, J. A.; Lawton, S. L.; Rubin, M. K. *Science* **1994**, *264*, 1910.
(39) Wu, P.; Tatsumi, T. *J. Catal.* **2003**, *214*, 317.
(40) Wu, P.; Fan, W.; Nuntasri, D.; Tatsumi, T. *Stud. Surf. Sci. Catal.* **2004**, *154*, 2581.
(41) Wu, P.; Tatsumi, T.; Komatsu, T.; Yashima, T. *J. Catal.* **2001**, *202*, 245.
(42) Wang, L.; Liu, Y.; Xie, W.; Wu, H.; Li, X.; He, M. Y.; Wu, P. *J. Phys. Chem. C* **2008**, *112*, 6132.
(43) *Spartan '10*; Wavefunction, Inc.: Irvine, CA. Except for molecular mechanics and semi-empirical models, the calculation methods used in *Spartan* have been documented in Shao, Y.; Molnar, L. F.; Jung, Y.; Kussmann, J.; Ochsenfeld, C.; Brown, S. T.; Gilbert, A. T. B.; Slipchenko, L. V.; Levchenko, S. V.; O'Neill, D. P.; DiStasio, R. A.; Lochan, R. C.; Wang, T.; Beran, G. J. O.; Besley, N. A.; Herbert, J. M.; Lin, C. Y.; Van Voorhis, T.; Chien, S. H.; Sodt, A.; Steele, R. P.; Rassolov, V. A.; Maslen, P. E.; Korambath, P. P.; Adamson, R. D.; Austin, B.; Baker, J.; Byrd, E. F. C.; Dachsel, H.; Doerksen, R. J.; Dreuw, A.; Dunietz, B. D.; Dutoi, A. D.; Furlani, T. R.; Gwaltney, S. R.; Heyden, A.; Hirata, S.; Hsu, C.-P.; Kedziora, G.; Khalliulin, R. Z.; Klunzinger, P.; Lee, A. M.; Lee, M. S.; Liang, W. Z.; Lotan, I.; Nair, N.; Peters, B.; Proynov, E.I.; Pieniazek, P. A.; Rhee, Y. M.; Ritchie, J.; Rosta, E.; Sherrill, C. D.; Simmonett, A. C.; Subotnik, J. E.; Woodcock, H. L.; Zhang, W.; Bell, A. T.; Chakraborty, A. K.; Chipman, D. M.; Keil, F. J.; Warshel, A.; Hehre, W. J.; Schaefer, H. F.; Kong, J.; Krylov, A. I.; Gill, P. M. W.; Head-Gordon, M. *Phys. Chem. Chem. Phys.* **2006**, *8*, 3172.
(44) Neese, F. *Comput. Mol. Sci.* **2012**, *2*, 73.
(45) Wachters, A. J. H. *J. Chem. Phys.* **1970**, *52*, 1033.
(46) Wachters, A. J. H. *IBM Tech. Rept. RJ584*; IBM: Armonk, NY, 1969.
(47) Bauschlicher, C. W.; Langhoff, S. R., Jr.; Barnes, L. A. *J. Chem. Phys.* **1989**, *91*, 2399.
(48) Wu, P.; Tatsumi, T. *J. Phys. Chem. B* **2002**, *106*, 748.
(49) Ricchiardi, G.; Damin, A.; Bordiga, S.; Lamberti, C.; Spanò, G.; Rivetti, F.; Zecchina, A. *J. Am. Chem. Soc.* **2001**, *123*, 11409.
(50) Kumar, R.; Sithambaram, S.; Suib, S. L. *J. Catal.* **2009**, *262*, 304.
(51) Zhou, L.; Xu, J.; Miao, H.; Wang, F.; Li, X. *Appl. Catal., A* **2005**, *292*, 223.
(52) Bellussi, G.; Carati, A.; Clerici, M. G.; Maddinelli, G.; Millini, R. *J. Catal.* **1992**, *133*, 220.
(53) Clerici, M. G.; Ingallina, P. *J. Catal.* **1993**, *140*, 71.
(54) Bordiga, S.; Damin, A.; Bonino, F.; Zecchina, A.; Spanò, G.; Rivetti, F.; Bolis, V.; Lamberti, C. *J. Phys. Chem. B* **2002**, *106*, 9892.
(55) Bordiga, S.; Damin, D.; Bonino, F.; Ricchiardi, G.; Lamberti, C.; Zecchina, A. *Angew. Chem., Int. Ed.* **2002**, *41*, 4734.
(56) Bordiga, S.; Damin, A.; Bonino, F.; Ricchiardi, G.; Zecchina, A.; Tagliapietra, R.; Lamberti, C. *Phys. Chem. Chem. Phys.* **2003**, *5*, 4390.
(57) Ratnasamy, P.; Srinivas, D.; Knozinger, H. *Adv. Catal.* **2004**, *48*, 1.
(58) Wang, L.; Xiong, G.; Su, J.; Li, P.; Guo, H. *J. Phys. Chem. C* **2012**, *116*, 9122.
(59) Karlsen, E.; Schöffel, K. *Catal. Today* **1996**, *32*, 107.
(60) Sinclair, P. E.; Catlow, C. R. A. *J. Phys. Chem. B* **1999**, *103*, 1084.
(61) Barker, C. M.; Gleeson, D.; Kaltsoyannis, N.; Catlow, C. R. A.; Sankara, G.; Thomas, J. M. *Phys. Chem. Chem. Phys.* **2002**, *4*, 1228.
(62) To, J.; Sokol, A. A.; French, S. A.; Catlow, C. R. A. *J. Phys. Chem. C* **2008**, *112*, 7173.
(63) Bordiga, S.; Bonino, F.; Damin, A.; Lamberti, C. *Phys. Chem. Chem. Phys.* **2007**, *9*, 4854.
(64) Yoon, C. Y.; Hirsekorn, K. F.; Neidig, M. L.; Yang, X.; Tilley, T. D. *ACS Catal.* **2011**, *1*, 1665.
(65) Wells, D. H.; Nicholas Delgass, W.; Thomson, K. T. *J. Am. Chem. Soc.* **2004**, *126*, 2956.
(66) Gallo, E.; Bonino, F.; Swarbrick, J. C.; Petrenko, T.; Piovano, A.; Bordiga, S.; Gianolio, D.; Groppo, E.; Neese, F.; Lamberti, C.; Glatzel, P. *ChemPhysChem* **2013**, *14*, 79.
(67) Chaudhari, K.; Bal, R.; Srinivas, D.; Chandwadkar, A. J.; Sivasanker, S. *Microporous Mesoporous Mater.* **2001**, *50*, 209.
(68) Tuel, A.; Diab, J.; Gelin, P.; Dufaux, M.; Dutel, J. E.; Taárit, B. Y. *J. Mol. Catal.* **1990**, *63*, 95.
(69) Petit, C.; Favre-Reguillon, A.; Albela, B.; Bonneviot, L.; Mignani, G.; Lemaire, M. *Organometal.* **2009**, *28*, 6379.
(70) Bonoldi, L.; Busetto, C.; Congiu, A.; Marra, G.; Ranghino, G.; Salvalaggio, M.; Spanò, G.; Giamello, E. *Spectrochim. Acta, Part A* **2002**, *58*, 1143.
(71) Zhao, Q.; Bao, X.-H.; Wang, Y.; Lin, L.-W.; Li, G.; Guo, X.-W.; Wang, X.-S. *J. Mol. Catal. A: Chem.* **2000**, *157*, 265.
(72) Zhuang, J.; Yang, G.; Ma, D.; Lan, X.; Liu, X.; Han, X.; Bao, X.; Mueller, U. *Angew. Chem., Int. Ed.* **2004**, *43*, 6377.
(73) Srinivas, D.; Manikandan, P.; Laha, S. C.; Kumar, R.; Ratnasamy, P. *J. Catal.* **2003**, *217*, 160.
(74) Heinrich, S.; Plettig, M.; Klemm, E. *Catal. Lett.* **2011**, *141*, 251.
(75) Clerici, G. *Top. Catal.* **2001**, *15*, 257.
(76) ΔG values have been calculated for the gas phase, a situation that is far from reality for our liquid-phase system. Therefore, these values have to be treated with care.
(77) Clerici, G. *Metal Oxide Catalysis*; Wiley VCH: Hoboken, NJ, 2009, Vol. 2, p 705.
(78) Murphy, E. F.; Ferri, D.; Baiker, M.; Van Doorslaer, S.; Schweiger, A. *Inorg. Chem.* **2003**, *42*, 2559.